Phyllosphere Microbiome in Response to Citrus Melanose

Pudong Li
Zhejiang University

Jianping Xu
McMaster University

Zhengyi Wang
Zhejiang University

Hongye Li (✉ hyli@zju.edu.cn)
Zhejiang University   https://orcid.org/0000-0002-6048-1745

Research

Abstract

Background: Like microbiomes in the rhizosphere, phyllosphere microbiomes can have an important role in plant growth and health. However, whether and how the phyllosphere microbiomes respond to the invasion of pathogens is not well understood. In this study, we address this question using the citrus phyllosphere-associated microbiome as a model.

Results: Through DNA metabarcoding (16S for bacteria and ITS for fungi) and shotgun metagenomic sequencing, we found that phyllosphere microbiomes in different ecological habitats (epiphytes and endophytes) responded differently to melanose disease caused by the fungal pathogen *Diaporthe citri* on citrus (*Citrus unshiu*) leaves. We observed that citrus phyllosphere-associated microbiome responded to the melanose disease in five ways: (1) increasing microbial richness; (2) reducing community evenness; (3) enriching selected microbes; (4) enhancing microbial interactions; and (5) enriching functional features involved in metabolism and fungal cell wall degrading.

Conclusions: Our study revealed how phyllosphere microbiomes in the epiphytic and endophytic habitats differ between diseased and healthy leaves. Based on the differences at both the taxonomic and functional levels, we propose a general conceptual paradigm to describe the different microbial community assembly processes for the phyllosphere microbiome in response to leaf disease and how such processes impact plant health. Our results provide novel insights for understanding the contributions of the phyllosphere microbial community response during pathogen invasion.

Background

Like the rhizosphere, the phyllosphere (aboveground part of terrestrial plants) is an important niche of the plant [1]. The phyllosphere is inhabited by diverse microbes, with some microbes living on the surface of plants as epiphytes and others colonizing inside leaves as endophytes [2]. These microbes, which mostly include bacteria and fungi, form microbial communities that are associated with phyllosphere habitats. The microbial communities associated with the phyllosphere are collectively called the phyllosphere microbiome [3].

A number of studies have demonstrated that phyllosphere microbes can provide plants with nutrients, modulate plant growth, and maintain plant health through either competition with pathogens or induction of plant resistance against pathogens [4]. However, most of these studies have focused on the interactions between a few members of the phyllosphere microbiome. As a major line of defense against infectious diseases, a clear understanding of how the phyllosphere microbiome responds to infections can help us develop better biocontrol and prevention strategies against diseases. However, almost nothing is known about how the phyllosphere microbiome responds to infections at present. The rapid development of high-throughput sequencing makes it possible to explore the dynamic changes of phyllosphere microbial communities, including functional differences due to leaf infections.

In this study, we investigated and compared the phyllosphere microbiomes between diseased and healthy leaves from citrus trees under natural field conditions. Different from most crops that have been investigated for phyllosphere microbiomes, citrus trees are perennial plants and have evergreen leaves with relatively stable phyllosphere phenotypes. Consequently, analyzing their phyllosphere microbiome could provide new insights about the stability of phyllosphere communities in perennial plants. Through metabarcoding (16S for bacteria and ITS for fungi) and shotgun metagenomic sequencing (Fig. 1), here we investigated the variations of phyllosphere microbial communities between healthy leaves and leaves infected by *Diaporthe citri*, a fungal pathogen that causes spot-like lesions in citrus leaves known as melanose disease (Additional file 1: Fig. S1) [5]. The aim of this study was to explore the microbial community assembly processes including microbial diversity, network structure, and functional enrichment of the phyllosphere in response to leaf disease.

Results

Structure of the citrus phyllosphere microbiome

To explore variation in the phyllosphere microbiome when facing the invasion of pathogens, we generated a microbial community profile for each sample using 16S and ITS metabarcoding data. In total, we obtained 6,770,888 sequences from phyllosphere samples. After denoising, removing low-quality and chimeric sequences with DADA2 [6], a range of amplicon sequence variants (ASVs) were obtained for the four sample types epiphytic bacteria, epiphytic fungi, endophytic bacteria, and endophytic fungi, with 2590, 664, 472 and 245 ASVs respectively based on 20 replicates of each (Additional file 2: Table S1).

In this study, the Richness index (Observed ASVs) and Evenness index (Pielou's Evenness) were used to assess the alpha diversity for each of the four microbiomes. Our results showed that the phyllosphere microbiomes from different ecological niches (epiphytes and endophytes) have different patterns of microbial diversity. Specifically, epiphytes on diseased leaves had greater microbial richness for both bacteria and fungi (Kruskal-Wallis; $p < 0.05$) than those on healthy leaves. However, no significant difference was found between diseased and healthy leaves in their endophytes (Fig. 2 and Additional file 2: Table S3). Interestingly, almost half of the total bacterial ASVs (48.6%) were found only in the epiphytic microbiome of the diseased leaves while only 14.4% were unique to the endophytes (Fig. 3c and Additional file 1: Fig. S2c). Most of the shared bacterial ASVs (75.0%) between the healthy and diseased leaves in their epiphytes belonged to the following top five classes: Alphaproteobacteria (26.8%), Gammaproteobacteria (20.8%), Bacteroidia (13.3%), Bacilli (8.0%) and Actinobacteria (6.3%). In contrast, 45.7% of the unique bacterial ASVs in the epiphytic microbiome of the diseased leaves belonged to these top five classes of Alphaproteobacteria (12.4%), Gammaproteobacteria (11.6%), Thermoleophilia (9.8%), Subgroup 6 (5.9%) and Actinobacteria (5.9%). In the endophytic microbiomes, no significant difference of microbial richness was found between the healthy and diseased leaves. However, the community evenness of both bacterial and fungal communities in the diseased leaves were significantly lower (Kruskal-Wallis; $p < 0.01$) than those in the healthy leaves (Fig. 2 and Additional file 2: Table S3). Interestingly, most of the differential ASVs in the endophytes of diseased leaves were those that showed

depleted distributions, contrary to that in the epiphytic microbiome (Fig. 3a, d and Additional file 1: Fig. S2a, d). Furthermore, there was no significant difference in the Evenness index of epiphytes between the healthy and diseased leaves for either bacteria or fungi (Fig. 2 and Additional file 2: Table S3).

Unconstrained principal coordinate analysis (PCoA) of the Bray-Curtis matrix was used to investigate patterns of separation between microbial communities, and differential microbial analysis was used to assess the enrichment at ASVs and genus level. Our analyses found that the epiphytic and endophytic microbiomes from leaves have different microbial community assemblies. Specifically, PCoA indicated that the bacterial communities between the diseased and healthy leaves differed significantly in both the epiphytic (PERMANOVA; $P < 0.05$) and endophytic (PERMANOVA; $P < 0.01$) habitats. In contrast, the fungal community assemblies did not show significant differences between the diseased and healthy leaves in the epiphytic habitat, while their endophytic communities exhibited significant differences (PERMANOVA; $P < 0.001$) (Fig. 2 and Additional file 2: Table S3). Moreover, a higher percentage of bacterial ASVs than that of the fungal ASVs showed significant differences in epiphytes between the diseased and healthy groups (Fig. 3a, d). Among them, 118 bacterial ASVs (22% of total ASVs) were significantly different (Wilcoxon test; $P < 0.05$), among which 109 were enriched and 9 were depleted in the diseased leaves (Fig. 3a). By contrast, 27 fungal ASVs (13% of total ASVs) were significantly different (Wilcoxon test; $P < 0.05$), among which 19 were enriched and 8 were depleted in the disease leaves (Fig. 3d).

Further taxonomic analysis of 16S rRNA profiling at the genus level showed that the enriched bacteria in the epiphytic habitat of the diseased leaves belonged to Alphaproteobacteria, Gammaproteobacteria and the other 8 classes (Additional file 2: Table S5). In comparison, all enriched bacteria in the endophytic habitat of diseased leaves belonged to Alphaproteobacteria (Additional file 2: Table S5). Moreover, Sphingomonas exhibited significant enrichment in both the epiphytic and endophytic habitats (Fig. 3b and Additional file 1: Fig. S2b). Interestingly, while enriched in the endophytic habitat, *Methylobacterium* was depleted in the epiphytic habitat of the diseased leaves (Fig. 3b and Additional file 1: Fig. S2b). Overall, the differentially distributed bacteria were mainly attributed to the following two functional categories: "plant growth promoting" (e.g. *Bacillus*, *Methylobacterium* and *Sphingomonas*) [7–9] and "plant metabolism-related" (e.g. *Methylocella* and *Zymobacter*) (Additional file 2: Table S5) [10, 11].

In contrast, taxonomic analysis of ITS profiling at the genus level showed that the enriched fungi in both the epiphytic and endophytic habitats of the diseased leaves belonged to four classes: Sordariomycetes, Eurotiomycetes, Dothideomycetes and Agaricomycetes (Additional file 2: Table S5). Specifically, the genus *Colletotrichum* exhibited significant enrichment in both the epiphytic and endophytic habitats of the diseased leaves (Fig. 3e and Additional file 1: Fig. S2e). In contrast, *Alternaria* and *Nigrospora* exhibited significant depleting in both the epiphytic and endophytic habitats (Fig. 3e and Additional file 1: Fig. S2e). Functionally, most of the differentially distributed fungi belonged to "potential plant pathogens" (e.g. *Colletotrichum*, *Alternaria* and *Nigrospora*) (Additional file 2: Table S5) [12–14]. Of these, *Colletotrichum* [13] and *Alternaria* [12] contain known pathogens of citrus. Interestingly, 5/6 depleted

fungi in the epiphytic habitat of diseased leaves also belonged to "potential plant pathogens" (Additional file 2: Table S5).

A large number of "Bacteria-Bacteria" interactions in epiphytes were intensified in diseased leaves

To explore whether changes in microbial community assemblies were accompanied by changes in microbial interactions, we performed co-occurrence network analysis to uncover potential associations and complexity of connections within the phyllosphere microbiome in response of disease. This was followed by estimating the topological properties of the co-occurrence networks to identify differences between the diseased and healthy groups. The co-occurrence networks were analyzed by Spearman correlations based on quantitative data of ASVs.

Our co-occurrence network analysis revealed increased complexity in the diseased condition compared with the healthy condition (Fig. 4 and Additional file 1: Fig. S3). A previous study showed that highly connected networks can form and strengthened when microbiomes face environmental disturbance, such as pathogen invasion [15]. Furthermore, the number of negative edges (negative interactions) of the networks in the disease group were higher than that in the healthy group (both in epiphytes and endophytes), suggesting that pathogen invasion intensified the microbial competition within both niches (Fig. 4 and Additional file 1: Fig. S3). Interestingly, in addition to increasing the interaction between the bacteria and fungi, a large number of "Bacteria-Bacteria" positive interactions in epiphytes were also intensified in the diseased leaves, indicating that the epiphytic bacteria might strengthen interactions in response to the disease (Fig. 4 and Additional file 2: Table S6).

Our topological analysis of networks provided further insights into the variation of interactions. In epiphytes, the network of the diseased group presented a higher number of connections per node (average degree = 6.20) than that in the healthy group (4.39), indicating a highly connected microbial community in the diseased leaves. Furthermore, when nodes from the fungi were removed, the number of connections per node among bacteria increased in the epiphytic habitat of the diseased leaves (average degree = 7.01) while that in the healthy group decreased (3.13). The results of this analyses further indicated intensified "Bacteria - Bacteria" associations in the epiphytic habitat of diseased leaves (Additional file 2: Table S6).

Numbers of metabolism-related and glycoside hydrolase genes were enriched in the epiphytic microbiome of diseased leaves

To further explore the role of phyllosphere microbiome when facing pathogen invasion, especially on its impact on the interactions in the epiphytic habitat (Fig. 4), we performed shotgun metagenomic sequencing of the epiphytic microbiome. The combined datasets of the diseased and healthy groups contained a total of 133.8 Gbp of raw reads. Quality filtering and removal of plant-derived reads resulted in 79.4 Gbp microbial reads. In total, 7,621,585 putative protein-coding genes were predicted from the

assembly. After clustering sequences at 95% identity, 5,592,809 non-redundant genes were generated (Additional file 2: Table S2).

Of the genes retrieved from the shotgun metagenomic data, 28 to 58% were assigned to a known function (Additional file 2: Table S2). Functional annotations were obtained for approximately 53% of non-redundant genes by aligning to the KEGG database and generated 15,423 KOs (GhostKOALA Score > 10). Based on KEGG level 1 pathway annotations, KOs could be classified into metabolism (33.7%), genetic information processing (14.6%), cellular processes (11.2%), environmental information processing (10.2%) and organismal systems (9.7%) (Additional file 2: Table S7). Differential enrichment analysis (DESeq2; Fold Change > 2 or < -2, P < 0.05, FDR < 0.1) of the epiphytic microbiomes between the diseased and healthy leaves revealed that 1283 KOs were enriched in the diseased samples, whereas 498 KOs were depleted (Fig. 5a). Furthermore, we found that the enriched KOs belonged mainly to metabolism-related pathways. Specifically, a large number of enriched KOs were involved in pathways of unclassified-metabolism (131 KOs), carbohydrate metabolism (124 KOs), amino acid metabolism (77 KOs), metabolism of cofactors and vitamins (56 KOs), energy metabolism (50 KOs) and xenobiotics biodegradation and metabolism (32 KOs), which represent 6 of top 10 pathways with enriched KOs (Fig. 5b and Additional file 2: Table S8). Consistent with network inferences (Fig. 4), this provides further evidence that the metabolism-based interactions of epiphytic microbes were dramatically enhanced when infected with melanose disease. In addition to metabolism-related pathways, enriched KOs in the diseased group also include those involved in "Plant-Microbe and "Microbe-Microbe" signal interactions, including the pathways of ABC transporters (61 KOs), two-component system (56 KOs), quorum sensing (19 KOs) and bacterial secretion system (16 KOs) (Additional file 2: Table S9). Together, these results indicated that increased epiphytic microbiome-mediated molecular communications among microbes and/or between microbes and plants in response to disease.

For more detailed resolution of specific functions associated with metabolism-related pathways, we searched for carbohydrate-active enzymes (CAZy) within the shotgun metagenomic data (Fig. 6 and Additional file 2: Table S10). A total of 428 CAZy gene families were identified and annotated with auxiliary activities (AA), glycoside hydrolases (GH), glycosyltransferases (GT), polysaccharide lyases (PL), and carbohydrate esterases (CE), as well as carbohydrate-binding modules (CBM). Differential enrichment analysis (DESeq2; Fold Change > 2 or < -2, P < 0.05, FDR < 0.1) of the epiphytic microbiomes between the diseased and healthy groups revealed that 35 CAZy gene families were enriched in the diseased group, whereas 5 CAZy gene families were depleted. Among them, most of the enriched CAZy gene families belonged to glycoside hydrolases (25 CAZy gene families). Many of these glycoside hydrolase families are associated with degradation of fungal cell wall components, including glucans (GH5_13, GH5_27, GH13_30, GH13_39 and GH74), mannans (GH5_13, GH5_27, GH99, GH130 and GH164) and chitosanase (GH5_13, GH5_27 and GH8), suggesting the epiphytic microbiome might be involved with disease suppression [16].

Taxonomic diversity of the phyllosphere microbiome

In this study, we used shotgun metagenomic data from the diseased group to compare microbial diversity between epiphytes and endophytes. Taxonomic annotation was assigned at reads level using NCBI nr database. Our analyses revealed that the epiphytic and endophytic niches had different microbial assemblies, suggesting their potential functional differences (Fig. 7).

Specifically, bioinformatic analyses of the shotgun metagenome sequences of the epiphytic microbes revealed that 66.7, 33.1, 0.2 and 0.1% of the reads corresponded to Bacteria, Fungi, Archaea and Viruses, respectively. By contrast, Bacteria (95.2%) were the predominant group among the endophytic microbes, with small fractions of Fungi (4.4%), Archaea (0.3%), and Viruses (0.2%). The dominance of bacteria in endophytes was largely attributed to *Acinetobacter* (47.2%). The shared bacteria between epiphytes and endophytes in the top 10 genera by relative abundance including *Acinetobacter*, *Bacillus*, *Mesorhizobium*, *Paenibacillus*, *Pseudomonas* and *Streptomyces*. In contrast, the shared fungi in the top 10 genera by relative abundance including *Aspergillus*, *Rachicladosporium*, *Fusarium* and *Colletotrichum* (Fig. 7). Moreover, 0.29% of the fungal sequence reads in the epiphytic habitat corresponded to the pathogen-related sequences (annotated as *Diaporthe* sp.), compared to 0.18% in the endophytic habitat.

De novo assembly of epiphytic bacterial genomes

Next, we attempted to identify epiphytic bacterial strains that might contribute to microbiome-related disease responses by binning genomes using the metagenome-assembled genome (MAG) extraction approach (Fig. 8a). After refinement and re-assembly, 24 bins (draft genomes) had completeness > 70% and contamination < 10% (Additional file 1: Fig. S4-6). Twelve of the 24 bins were enriched in the diseased leaves (Fold Change > 2), with bin 1 (Methylobacteriaceae) being the most abundant in epiphytes (Additional file 2: Table S11). Interestingly, 4/5 Sphingomonadaceae bins (bin 3, bin 11, bin 13 and bin 19) were enriched in the diseased leaves (Fig. 8b), consistent with our metabarcoding data (Fig. 3b), and suggesting a potential role for Sphingomonadaceae bacteria in host response to pathogen invasion on the citrus leaves. All four bins of Sphingomonadaceae were enriched by > 25-fold in diseased leaves over the healthy group (Additional file 2: Table S11). Among these four bins, bin 13 had the highest quality (completeness = 90.52%, contamination = 7.46%, N50 = 16,164). The assembled genome was comprised of 260 contigs with a total length of 2.62 Mb. We named this genome CPG1, short for citrus phyllosphere genome 1. We determine the taxonomy of CPG1 using Taxator-tk [17] and PhyloPhlAn [18], both annotated the genome to *Sphingomonas* sp. (Additional file 2: Table S11).

To better understand the putative functions of Sphingomonadaceae in the phyllosphere, we selected CPG1 as a representative genome for subsequent analyses based on the phylogenetic tree (Fig. 8b). As reported in previous studies, *Sphingomonas* may be involved in inducing plant defence signaling pathways and in inhibiting the growth and virulence of pathogens, which could help reduce host plant damages in the phyllosphere [19]. Here, analyses of the binned genomes revealed that microbes enriched in diseased leaves contained more gene families associated with fungal cell wall-degrading enzymes (CWDEs), similar to results in shotgun reads (Fig. 6). Specifically, we found that CPG1 contains 12 CAZy protein family related to fungal CWDEs, suggesting that the enrichment of the genus *Sphingomonas* in the diseased leaves is likely associated with antifungal functions. Furthermore, glycoside hydrolases

(GH99, GH74 and GH164) were not found in any of these 24 bins, which related to the degradation of glucans or mannans. The results suggest that the enrichment of CWDEs genes in diseased leaves was likely driven by multiple microbes, emphasizing the overall role of the microbial community in response to plant diseases (Additional file 2: Table S11).

Discussion

The microbiome has long been recognized as an essential part of the crop ecosystem, which is closely linked to the growth of plants and resistance to diseases [20]. In recent years, the rhizosphere microbiome (underground part) has been extensively studied, while the phyllosphere microbiome (aboveground part) has been less studied. In addition, most plants investigated so far are either model plants such as *Arabidopsis thaliana* or annual crops. In this research, we used citrus trees for our investigation. These trees are perennial plants and have evergreen leaves with relatively stable phyllosphere phenotypes compared the most crops. Our research provided a systematic description on how the phyllosphere microbiome in citrus responded to invasion by the fungal pathogen *Diaporthe citri* [5] (Additional file 1: Figure S1) and revealed new insights into relevance of the phyllosphere microbiome to the health of a perennial plant.

In epiphytic habitat, we found that the diseased leaves had significantly greater microbial richness than that on healthy leaves (Fig. 2). Similar to the pattern observed for the rhizosphere microbes responding to disease invasion in other plants [21], the phyllosphere microbiome also had new microbial recruits to perform infection-response functions (Fig. 9). The significant increase of microbial diversity has led to a dramatic strengthening of interactions between microbes (especially among bacteria) in the diseased phyllosphere (Fig. 4 and Additional file 1: Figure S3). Indeed, the strengthened interactions between certain microbes have been associated with improved plant health [15]. Moreover, infections have shown capable of inducing assemblage of a plant-beneficial microbiome [22]. Our observation that several growth-promoting beneficial microbes were enriched in the epiphyte of diseased leaves is consistent with previous reports (e.g. *Sphingomonas*, *Rhizobiaceae* and *Coniothyrium*) (Fig. 9 and Additional file 2: Table S5) [8, 9, 23]. Specifically, our shotgun metagenomic data identified a large number of enriched genes related to metabolism and glycoside hydrolases in the epiphytic habitat in the diseased leaves (Figs. 5 and 6). Together, these results suggest that infection by the fungal pathogen *D. citri* induced new microbial recruitments and the enrichments of selected groups of microorganisms and genes associated with metabolism and antifungal activities.

Recent studies support that variations in plant microbiomes are not merely the results of their passive responses to external stresses but rather an active process involving selectively recruiting and enriching certain groups of microbes [19]. Our results highlight the essential role of epiphytes in resistance to pathogen invasion, similar to that found in the rhizosphere of several plants such as tomato and common bean [24–26]. In the rhizosphere, the response of microbial community assembly to pathogen infection was primarily driven by changes in root exudate [27]. Whether changes in leaf exudates caused by infection are responsible for changes in phyllosphere microbiome requires further study.

In the endophytic habitat, we did not observe obvious differences in microbial richness between the healthy and diseased leaves. However, we found that the community evenness was significantly reduced in diseased leaves (Fig. 2, 8). This result is similar to recent studies indicating that dysbiosis of endophytic microbiome in the phyllosphere caused the leaves to exhibit non-pathogenic symptoms of the disease [28], suggesting that the structure of the endophytic microbiome could play a key role in maintaining plant health. However, how diseases mediated by pathogenic invasions are related to dysbiosis of the endophytic microbiome remains to be further studied. Recent studies support that the endophytes constitute a second microbial layer of plant defense [29]. Our study revealed that several plant growth-promoting bacteria (PGPB) (e.g. *Methylobacterium* and *Sphingomonas*) [7, 9] were enriched in endophytes in response to *D. citri* infection (Fig. 9, Additional file 1: Fig. S2b and Additional file 2: Table S5). The process of responding to infections by enriching beneficial endophytic microbes is likely to be proactive, similar to that observed in the rhizosphere where the pathogen could activate disease-suppressive functions in the endophytic root microbiome [30].

Aside from evidence for the recruitment of new microbes from the environment to the epiphytic habitat in response to *D. citri* infection, there is also evidence for recruitment from the epiphytic to the endophytic habitat (Fig. 9). In our study, in the diseased leaves, *Methylobacterium* was depleted in epiphytes but enriched in endophytes (Fig. 3b, Additional file 1: Fig. S2b and Additional file 2: Table S5), suggesting a potential transfer. Disease-mediated microbial transfers between closely related ecological niches have been proposed for the rhizosphere habitats [31]. *Methylobacterium* has been widely studied as PGPB that plays essential roles in plant health and disease suppression in the rhizosphere [32]. Together, these results suggest that increased colonization of beneficial microbes might be a general response of plants to infections.

In addition to enrichment of beneficial microbes, "potential plant pathogens" were also enriched in the phyllosphere of the diseased leaves (e.g. *Cyphellophora* and *Colletotrichum*) (Additional file 2: Table S5) [13, 33]. Recent studies found that attempts to explain the occurrence of diseases by identifying single pathogens often represented incomplete understanding of the true causes [34]. Instead, synergistic interactions among multiple microbial pathogens may represent the prevalent pattern in nature [35]. In our study, almost all of the depleted fungi (5/6) in epiphytic habitat of the diseased leaves were "potential plant pathogens" (Additional file 2: Table S5), further suggesting that microbial responses triggered by the invasion of one pathogen *D. citri* might suppress other, potentially synergistically acting groups of pathogens. This result consistent with our shotgun metagenomic evidence (numbers of fungal cell wall-degrading related gene families were enriched in the epiphytic habitat) (Fig. 6).

Overall, this study indicates that the phyllosphere microbial community likely adopts multiple strategies to respond to pathogenic invasions. At present, there relative contributions to host disease resistance or microbial pathogenesis are unclear and require further studies. Interestingly, the patterns of variation among the phyllosphere microbiomes found in this study have many similarities to the rhizosphere microbiomes in response to diseases in many plants [36]. Such a broad similarity suggests that phyllosphere microbiomes most likely represent the first line of defense against foliar diseases.

Conclusions

In this study, we explored how phyllosphere microbiomes in the epiphytic and endophytic habitats differ between diseased and healthy leaves at both the taxonomic and functional levels through metabarcoding and shotgun metagenomics approaches. We used multiple lines of evidence from "Microbial Structure to Network Interaction to Functional Annotation" to highlight the relevance of the phyllosphere microbiome for plant health. Based on the combined data, we propose a conceptual paradigm (Fig. 9) to describe the different microbial community assembly processes for the phyllosphere microbiome in response to leaf disease. Specifically, these processes include: (i) recruiting new microbes, (ii) enhancing interactions among bacteria and (iii) enriching selected microbes in the epiphytic habitat; (iv) decreasing the microbial community evenness and (v) enriching selected microbes in the endophytic habitat; (vi) transferring and enriching microbes from the epiphytic to the endophytic habitats.

Methods

Sample collection and DNA extraction

Two groups ("Healthy" and "Diseased") of leaf samples (around 1 year old) of *Citrus unshiu* (> 20 years old), commonly known as tangerine and Satsuma orange, were collected from an orchard (28.64 N, 121.17 E) in Zhejiang province, China. The diseased samples were identified based on visual symptoms (Additional file 1: Fig. S1). In total, > 200 leaves of the two groups were collected, placed in sterile plastic bags, and immediately transported to laboratory in an ice-box and stored at − 80 °C pending further processing.

To collect the epiphytic microbiome, 6−8 leaves were first transferred into a 250 mL conical flask containing 200 mL 0.01 M sterile phosphate buffered saline (PBS, 4 °C), and then subjected to sonication (15 min) and shaking (1 h, 200 rpm, 20 °C) to dislodge the epiphytic microbes from the leaf surface into the washing solution. The washing solution was filtered with 0.22 μm clean sterile cellulose membrane filter to capture all the microbes in the solution. The membrane was cut into pieces (2 × 2 mm) with sterilized scissors [37].

To collect the endophytic microbiome, the leaf samples washed using the procedure described above were surface sterilized by consecutive immersion for 1 min in 75% ethanol, 3 min in 1% sodium hypochlorite, and 30 s in 75% ethanol, followed with three rinses with sterile water. Subsequently, the treated leaves were freeze-dried using liquid nitrogen and homogenized using a sterilized pestle and mortar [37].

The leaf sample treated above (epiphytes or endophytes) represented one biological replicate, and was subjected to DNA extraction using the FastDNA® Spin Kit for Soil (MP Biomedical, Solon, OH, USA) according to the manufacturer's instructions. In total, four sample types were prepared, epiphytes from healthy leaves, endophytes from healthy leaves, epiphyte from diseased leaves, and endophyte from

diseased leaves. For each of the four sample types, ten biological replicates were prepared for metabarcoding sequencing, and three biological replicates for shotgun metagenomic sequencing.

DNA sequencing

For targeted metabarcoding sequencing, DNA fragments were amplified using primers targeting the 16S rDNA V4 region for bacteria and the ITS2 (Internal Transcribed Spacer 2) region for fungi (Additional file 2: Table S1). PCR reaction was done for each sample under the following conditions: 30 s at 98 °C; 35 cycles of denaturation at 98 °C for 10 s, annealing at 54 °C for 30 s, and extension at 72 °C for 45 s; final step 10 min at 72 °C [38]. The 25 μL PCR mixture contained 12.5 μL of Phusion® High-Fidelity PCR Master Mix (New England Biolabs Inc., Beverly, MA), 2.5 μL of each primer (1 μM) and 50 ng of template DNA. The PCR products were electrophoresed and stained with ethidium bromide for visualization. The specific DNA bands on the gel were excised and purified using Qiagen Gel Extraction Kit (Qiagen, Germany). Sequencing libraries were generated using TruSeq® DNA PCR-Free Sample Preparation Kit (Illumina, USA) following manufacturer's recommendations and then sequencing was conducted using the Illumina Novaseq 6000 Sequencer (Illumina, Inc., CA, USA).

For shotgun metagenomic sequencing, the extracted DNA samples were fractionated by ultrasound into approximately 350 bp fragments. The fragments were then used to construct the sequencing libraries using NEBNext® Ultra™ DNA Library Prep Kit for Illumina (NEB, USA). The libraries were sequenced using the Illumina Novaseq 6000 Sequencer (Illumina, Inc., CA, USA).

Bioinformatics analyses

For metabarcoding data, the reads were analyzed using QIIME 2 (Quantitative Insights Into Microbial Ecology 2, version 2019.7) and its plugins [39]. Briefly, to obtain amplicon sequence variants (ASVs), we first used DADA2 to remove low-quality reads and noises, including removing chimeras [6]. The ASVs were then assigned to taxonomy groupings based on comparisons with the UNITE database [40] for fungi and the Silva database [41] for bacteria using the q2-feature-classifier [42]. A small number of unclassified sequences were re-checked using BLAST with the NCBI nt database [43] to manually assign consensus taxonomy among the top hits with a minimum of 95% query coverage and 95% identity (Additional file 2: Table S4). Before the following diversity analysis, all samples were rarefied to the same number of reads. We calculated alpha diversity indices (Richness and Pielou's Evenness) and beta diversity metrics (Bray-Curtis) through the diversity plugin (q2-diversity).

For the shotgun metagenomic data, the raw reads were trimmed with the sliding window approach to generate the QC (Quality Control) reads using Trimmomatic [44]. Contamination of reads originating from the host plant were aligned to the nuclear genome of *Citrus unshiu* (GCA_002897195.1) [45], the plastid genomes of *Citrus sinensis* (NC_008334.1) [46] and *Citrus maxima* (NC_034290.1), and the mitochondrial genome of *Citrus sinensis* (NC_037463.1) [47] using Bowtie 2 [48]. After that, the concordantly mapped reads were removed to preserve the clean reads. To obtain the microbial reads and their taxonomic annotations, the clean reads were aligned against the NCBI nr (non-redundant) database [43] using Kraken 2 [49], and the reads that could not be aligned to bacteria, fungi, archaea or virus were filtered out.

The microbial reads from the epiphytic samples were pooled together for de novo assembly with MEGAHIT [50]. For the resulting contigs, ORF (Open Reading Frame) were predicted with Prodigal [51] in metagenomics mode and the non-redundant gene categories were generated using CD-HIT [52] with an identity cutoff of 95%. For gene annotation, DIAMOND [53] was used to annotate with nr database [43] and SWISS-PROT database [54]. For functional annotation, GhostKOALA [55] and DIAMOND were used to annotate with KEGG database [56] and CAZy (carbohydrate-active enzymes) database [57], respectively. Reads counts and TPM (transcripts per million) of each predicted gene were determined with Salmon [58]. Assembled metagenomic data were binned with MetaBAT 2 [59], MaxBin 2 [60] and CONCOCT [61]. Refinement and reassemble steps were then performed using the MetaWRAP [62] pipeline to combine and improve the results generated by the three binners (completion > 70% and contamination < 10%). We determine the taxonomy of each bin using Taxator-tk [17] against the NCBI nt database [43]. The bins were then quantified by Salmon [58] and predicted gene by Prodigal [51] with default parameters. All predicted genes from bins were annotated using dbCAN2 [63] against CAZy database [57]. A phylogenetic tree of bins was constructed using PhyloPhlAn [18] based on concatenated alignments of up to 400 ubiquitously conserved proteins and used the SGB (species-level genome bins) release [64] to assign to each genome bin its closest SGB. The thresholds of Mash distance we used to assign taxonomic labels were 0.05, 0.15, and 0.30 for species, genus, and families, respectively [64].

All statistical analyses were performed using specific packages in R version 3.6.3 (The R Foundation for Statistical Computing, Vienna, Austria), except for the network visualization, which was carried out in Cytoscape [65]. For significance testing, the P-value of Kruskal-Wallis was used to compare the difference of alpha diversity. PERMANOVA (Permutational Multivariate Analysis of Variance) was used to examine whether the sample groups harbored significantly different microbial community (i.e. beta diversity). Wilcoxon test was used to identify the statistical significance in differences of the relative abundance at different taxa between the groups. At the functional level, differentially abundant KOs (KEGG Orthologs) and CAZy gene families were identified using DESeq2 [66].

For network analyses, co-occurrence networks of the samples were performed using the Spearman correlation matrix constructed with the igraph package to assess the complexity of the interactions in phyllosphere microbiome [67]. The high relative abundances (> 0.01%) and statistically significant correlations ($P < 0.01$, Spearman's coefficient > 0.7 or < -0.7) among ASVs were included into the network analyses. To analyze the topology of the co-occurrence networks, we used a set of measures such as the numbers of edges, nodes and clusters, clustering coefficients, modularity, connectance, average degree, network diameter and average path length.

Declarations

Acknowledgements

insightful discussions; and Zhan-Xu Pu and Qun Wu for help with sample collection.

Availability of data and materials

The raw sequencing data (16S, ITS and shotgun metagenome) from this project are available in the NCBI Sequence Read Archive (SRA) database under BioProject PRJNA643596.

Authors' contributions

HL conceived and supervised the project; PDL and HL designed the experiment; PDL analyzed the data; PDL and HL wrote the manuscript; JX and ZW revised the manuscript. All authors read and approved the final manuscript.

Ethics approval and consent to participate

Not applicable.

Consent for publication

Not applicable.

Competing interests

The authors declare no competing interests.

References

1. Vorholt JA. Microbial life in the phyllosphere. Nat Rev Microbiol. 2012;10:828–40.
2. Leveau JH. A brief from the leaf: latest research to inform our understanding of the phyllosphere microbiome. Curr Opin Microbiol. 2019;49:41–9.
3. Remus-Emsermann MNP, Schlechter RO. Phyllosphere microbiology: at the interface between microbial individuals and the plant host. New Phytol. 2018;218:1327–33.
4. Stone BWG, Weingarten EA, Jackson CR. The Role of the Phyllosphere Microbiome in Plant Health and Function. Annual Plant Reviews online. 2018:533–56.
5. Huang F, Hou X, Dewdney MM, Fu Y, Chen G, Hyde KD, et al. Diaporthe species occurring on citrus in China. Fungal Divers. 2013;61:237–50.

6. Callahan BJ, McMurdie PJ, Rosen MJ, Han AW, Johnson AJ, Holmes SP. DADA2: High-resolution sample inference from Illumina amplicon data. Nat Methods. 2016;13:581–3.

7. Madhaiyan M, Suresh Reddy BV, Anandham R, Senthilkumar M, Poonguzhali S, Sundaram SP, et al. Plant growth-promoting Methylobacterium induces defense responses in groundnut (Arachis hypogaea L.) compared with rot pathogens. Curr Microbiol. 2006;53:270–6.

8. Berg G. Plant-microbe interactions promoting plant growth and health: perspectives for controlled use of microorganisms in agriculture. Appl Microbiol Biotechnol. 2009;84:11–8.

9. Khan AL, Waqas M, Asaf S, Kamran M, Shahzad R, Bilal S, et al. Plant growth-promoting endophyte Sphingomonas sp. LK11 alleviates salinity stress in Solanum pimpinellifolium. Environ Exp Bot. 2017;133:58–69.

10. Yanase H, Sato D, Yamamoto K, Matsuda S, Yamamoto S, Okamoto K. Genetic engineering of Zymobacter palmae for production of ethanol from xylose. Appl Environ Microbiol. 2007;73:2592–9.

11. Rahman MT, Crombie A, Chen Y, Stralis-Pavese N, Bodrossy L, Meir P, et al. Environmental distribution and abundance of the facultative methanotroph Methylocella. ISME J. 2011;5:1061–6.

12. Akimitsu K, Peever TL, Timmer LW. Molecular, ecological and evolutionary approaches to understanding Alternaria diseases of citrus. Mol Plant Pathol. 2003;4:435–46.

13. Huang F, Chen GQ, Hou X, Fu YS, Cai L, Hyde KD, et al. Colletotrichum species associated with cultivated citrus in China. Fungal Divers. 2013;61:61–74.

14. Wang M, Liu F, Crous PW, Cai L. Phylogenetic reassessment of Nigrospora: Ubiquitous endophytes, plant and human pathogens. Persoonia. 2017;39:118–42.

15. Faust K, Raes J. Microbial interactions: from networks to models. Nat Rev Microbiol. 2012;10:538–50.

16. Bowman SM, Free SJ. The structure and synthesis of the fungal cell wall. Bioessays. 2006;28:799–808.

17. Droge J, Gregor I, McHardy AC. Taxator-tk: precise taxonomic assignment of metagenomes by fast approximation of evolutionary neighborhoods. Bioinformatics. 2015;31:817–24.

18. Asnicar F, Thomas AM, Beghini F, Mengoni C, Manara S, Manghi P, et al. Precise phylogenetic analysis of microbial isolates and genomes from metagenomes using PhyloPhlAn 3.0. Nat Commun. 2020;11:2500.

19. Liu H, Brettell LE, Qiu Z, Singh BK. Microbiome-Mediated Stress Resistance in Plants. Trends Plant Sci. 2020.

20. Cordovez V, Dini-Andreote F, Carrión VJ, Raaijmakers JM. Ecology and Evolution of Plant Microbiomes. Annu Rev Microbiol. 2019;73:69–88.

21. Berendsen RL, Vismans G, Yu K, Song Y, de Jonge R, Burgman WP, et al. Disease-induced assemblage of a plant-beneficial bacterial consortium. ISME J. 2018;12:1496–507.

22. Zhalnina K, Louie KB, Hao Z, Mansoori N, da Rocha UN, Shi S, et al. Dynamic root exudate chemistry and microbial substrate preferences drive patterns in rhizosphere microbial community assembly.

Nat Microbiol. 2018;3:470–80.

23. Paulitz TC, Bélanger RR. Biological Control in Greenhouse Systems. Annu Rev Phytopathol. 2001;39:103–33.

24. de Zelicourt A, Al-Yousif M, Hirt H. Rhizosphere microbes as essential partners for plant stress tolerance. Mol Plant. 2013;6:242–5.

25. Mendes LW, Raaijmakers JM, de Hollander M, Mendes R, Tsai SM. Influence of resistance breeding in common bean on rhizosphere microbiome composition and function. ISME J. 2018;12:212–24.

26. Kwak MJ, Kong HG, Choi K, Kwon SK, Song JY, Lee J, et al. Rhizosphere microbiome structure alters to enable wilt resistance in tomato. Nat Biotechnol. 2018;36:1100–9.

27. Yuan J, Zhao J, Wen T, Zhao M, Li R, Goossens P, et al. Root exudates drive the soil-borne legacy of aboveground pathogen infection. Microbiome. 2018;6:156.

28. Chen T, Nomura K, Wang X, Sohrabi R, Xu J, Yao L, et al. A plant genetic network for preventing dysbiosis in the phyllosphere. Nature. 2020;580:653–7.

29. Dini-Andreote F, Endophytes. The Second Layer of Plant Defense. Trends Plant Sci. 2020;25:319–22.

30. Carrión VJ, Perez-Jaramillo J, Cordovez V, Tracanna V, De Hollander M, Ruiz-Buck D, et al. Pathogen-induced activation of disease-suppressive functions in the endophytic root microbiome. Science. 2019;366:606–12.

31. Zhang Y, Xu J, Riera N, Jin T, Li J, Wang N. Huanglongbing impairs the rhizosphere-to-rhizoplane enrichment process of the citrus root-associated microbiome. Microbiome. 2017;5:97.

32. Madhaiyan M, Poonguzhali S, Kang B-G, Lee Y-J, Chung J-B, Sa T-M. Effect of co-inoculation of methylotrophic Methylobacterium oryzae with Azospirillum brasilense and Burkholderia pyrrocinia on the growth and nutrient uptake of tomato, red pepper and rice. Plant Soil. 2009;328:71–82.

33. Gleason ML, Zhang R, Batzer JC, Sun G. Stealth Pathogens: The Sooty Blotch and Flyspeck Fungal Complex. Annu Rev Phytopathol. 2019;57:135–64.

34. Bass D, Stentiford GD, Wang HC, Koskella B, Tyler CR. The Pathobiome in Animal and Plant Diseases. Trends Ecol Evol. 2019;34:996–1008.

35. Brader G, Compant S, Vescio K, Mitter B, Trognitz F, Ma LJ, et al. Ecology and genomic insights into plant-pathogenic and plant-nonpathogenic endophytes. Annu Rev Phytopathol. 2017;55:61–83.

36. Chapelle E, Mendes R, Bakker PA, Raaijmakers JM. Fungal invasion of the rhizosphere microbiome. ISME J. 2016;10:265–8.

37. Yao H, Sun X, He C, Maitra P, Li XC, Guo LD. Phyllosphere epiphytic and endophytic fungal community and network structures differ in a tropical mangrove ecosystem. Microbiome. 2019;7:57.

38. Li PD, Jeewon R, Aruna B, Li HY, Lin FC, Wang HK. Metabarcoding reveals differences in fungal communities between unflooded versus tidal flat soil in coastal saline ecosystem. Sci Total Environ. 2019;690:911–22.

39. Bolyen E, Rideout JR, Dillon MR, Bokulich NA, Abnet CC, Al-Ghalith GA, et al. Reproducible, interactive, scalable and extensible microbiome data science using QIIME 2. Nat Biotechnol. 2019;37:852–7.

40. Nilsson RH, Larsson KH, Taylor AFS, Bengtsson-Palme J, Jeppesen TS, Schigel D, et al. The UNITE database for molecular identification of fungi: handling dark taxa and parallel taxonomic classifications. Nucleic Acids Res. 2019;47:D259-D64.

41. Quast C, Pruesse E, Yilmaz P, Gerken J, Schweer T, Yarza P, et al. The SILVA ribosomal RNA gene database project: improved data processing and web-based tools. Nucleic Acids Res. 2013;41:D590-6.

42. Bokulich NA, Kaehler BD, Rideout JR, Dillon M, Bolyen E, Knight R, et al. Optimizing taxonomic classification of marker-gene amplicon sequences with QIIME 2's q2-feature-classifier plugin. Microbiome. 2018;6:90.

43. Coordinators NR. Database resources of the National Center for Biotechnology Information. Nucleic Acids Res. 2014;42:D7–17.

44. Bolger AM, Lohse M, Usadel B. Trimmomatic: a flexible trimmer for Illumina sequence data. Bioinformatics. 2014;30:2114–20.

45. Shimizu T, Tanizawa Y, Mochizuki T, Nagasaki H, Yoshioka T, Toyoda A, et al. Draft Sequencing of the Heterozygous Diploid Genome of Satsuma (Citrus unshiu Marc.) Using a Hybrid Assembly Approach. Front Genet. 2017;8:180.

46. Bausher MG, Singh ND, Lee SB, Jansen RK, Daniell H. The complete chloroplast genome sequence of Citrus sinensis (L.) Osbeck var 'Ridge Pineapple': organization and phylogenetic relationships to other angiosperms. BMC Plant Biol. 2006;6:21.

47. Yu F, Bi C, Wang X, Qian X, Ye N. The complete mitochondrial genome of Citrus sinensis. Mitochondrial DNA Part B. 2018;3:592–3.

48. Langmead B, Salzberg SL. Fast gapped-read alignment with Bowtie 2. Nat Methods. 2012;9:357–9.

49. Wood DE, Lu J, Langmead B. Improved metagenomic analysis with Kraken 2. Genome Biol. 2019;20:257.

50. Li D, Liu CM, Luo R, Sadakane K, Lam TW. MEGAHIT: an ultra-fast single-node solution for large and complex metagenomics assembly via succinct de Bruijn graph. Bioinformatics. 2015;31:1674–6.

51. Hyatt D, Chen GL, LoCascio PF, Land ML, Larimer FW, Hauser LJ. Prodigal: prokaryotic gene recognition and translation initiation site identification. BMC Bioinf. 2010;11:119.

52. Fu L, Niu B, Zhu Z, Wu S, Li W. CD-HIT: accelerated for clustering the next-generation sequencing data. Bioinformatics. 2012;28:3150–2.

53. Buchfink B, Xie C, Huson DHJNm. Fast and sensitive protein alignment using DIAMOND. Nat Methods. 2015;12:59.

54. Boeckmann B, Bairoch A, Apweiler R, Blatter MC, Estreicher A, Gasteiger E, et al. The SWISS-PROT protein knowledgebase and its supplement TrEMBL in 2003. Nucleic Acids Res. 2003;31:365–70.

55. Kanehisa M, Sato Y, Morishima K. BlastKOALA and GhostKOALA: KEGG tools for functional characterization of genome and metagenome sequences. J Mol Biol. 2016;428:726–31.

56. Kanehisa M, Furumichi M, Tanabe M, Sato Y, Morishima K. KEGG: new perspectives on genomes, pathways, diseases and drugs. Nucleic Acids Res. 2017;45:D353-D61.

57. Lombard V, Golaconda Ramulu H, Drula E, Coutinho PM, Henrissat B. The carbohydrate-active enzymes database (CAZy) in 2013. Nucleic Acids Res. 2014;42:D490-5.

58. Patro R, Duggal G, Love MI, Irizarry RA, Kingsford C. Salmon provides fast and bias-aware quantification of transcript expression. Nat Methods. 2017;14:417–9.

59. Kang DD, Li F, Kirton E, Thomas A, Egan R, An H, et al. MetaBAT 2: an adaptive binning algorithm for robust and efficient genome reconstruction from metagenome assemblies. PeerJ. 2019;7:e7359.

60. Wu YW, Simmons BA, Singer SW. MaxBin 2.0: an automated binning algorithm to recover genomes from multiple metagenomic datasets. Bioinformatics. 2016;32:605–7.

61. Alneberg J, Bjarnason BS, de Bruijn I, Schirmer M, Quick J, Ijaz UZ, et al. Binning metagenomic contigs by coverage and composition. Nat Methods. 2014;11:1144–6.

62. Uritskiy GV, DiRuggiero J, Taylor J. MetaWRAP-a flexible pipeline for genome-resolved metagenomic data analysis. Microbiome. 2018;6:158.

63. Zhang H, Yohe T, Huang L, Entwistle S, Wu P, Yang Z, et al. dbCAN2: a meta server for automated carbohydrate-active enzyme annotation. Nucleic Acids Res. 2018;46:W95–101.

64. Pasolli E, Asnicar F, Manara S, Zolfo M, Karcher N, Armanini F, et al. Extensive Unexplored Human Microbiome Diversity Revealed by Over 150,000 Genomes from Metagenomes Spanning Age, Geography, and Lifestyle. Cell. 2019;176:649 – 62 e20..

65. Saito R, Smoot ME, Ono K, Ruscheinski J, Wang PL, Lotia S, et al. A travel guide to Cytoscape plugins. Nat Methods. 2012;9:1069–76.

66. Love MI, Huber W, Anders S. Moderated estimation of fold change and dispersion for RNA-seq data with DESeq2. Genome Biol. 2014;15:550.

67. Barberan A, Bates ST, Casamayor EO, Fierer N. Using network analysis to explore co-occurrence patterns in soil microbial communities. ISME J. 2012;6:343–51.
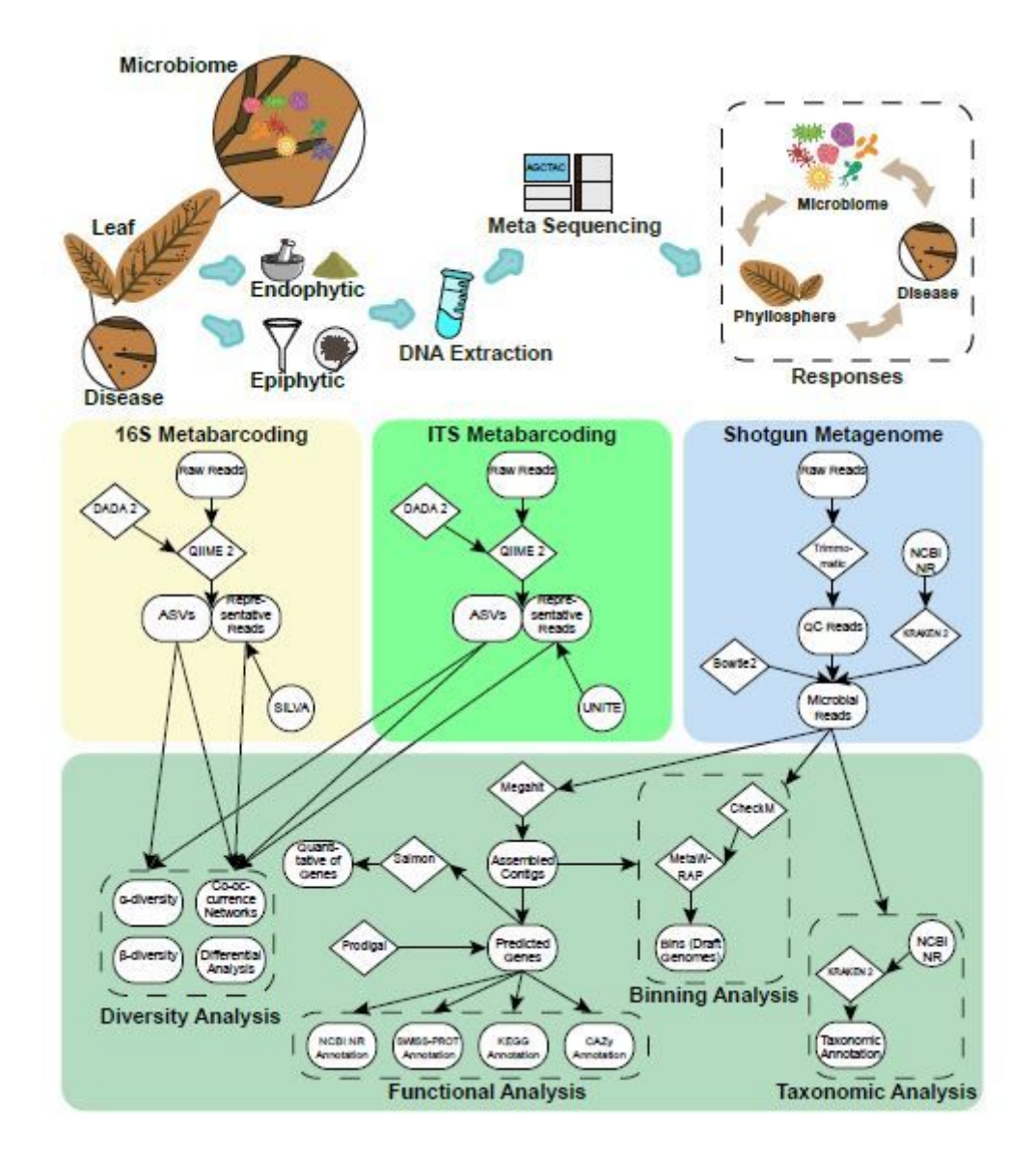
Figures

Figure 1

A workflow for separation, DNA extraction, and sequencing of the phyllosphere microbiomes. Schematic representation of the bioinformatic tools used for analyzing the metabarcoding and shotgun metagenomic data.
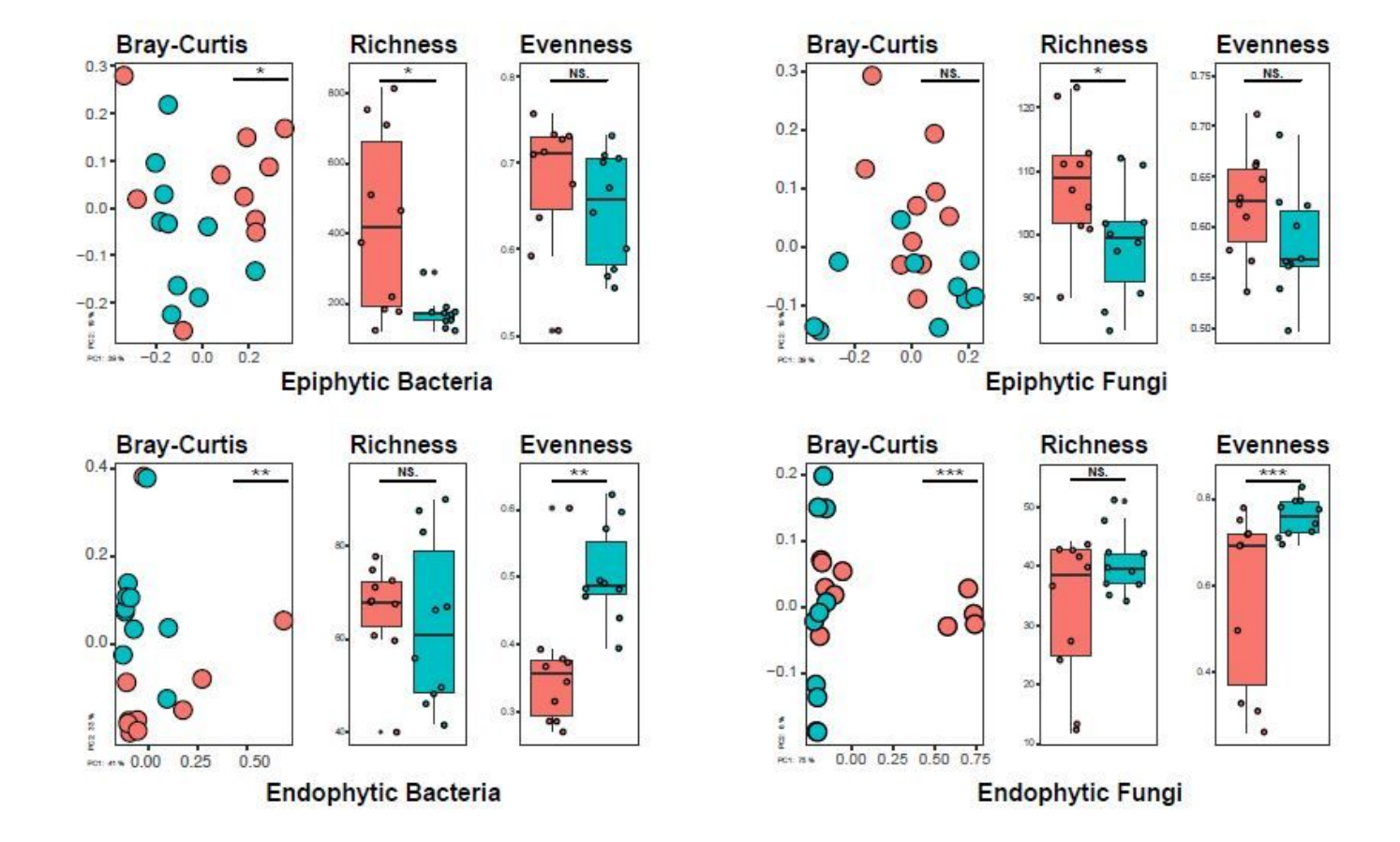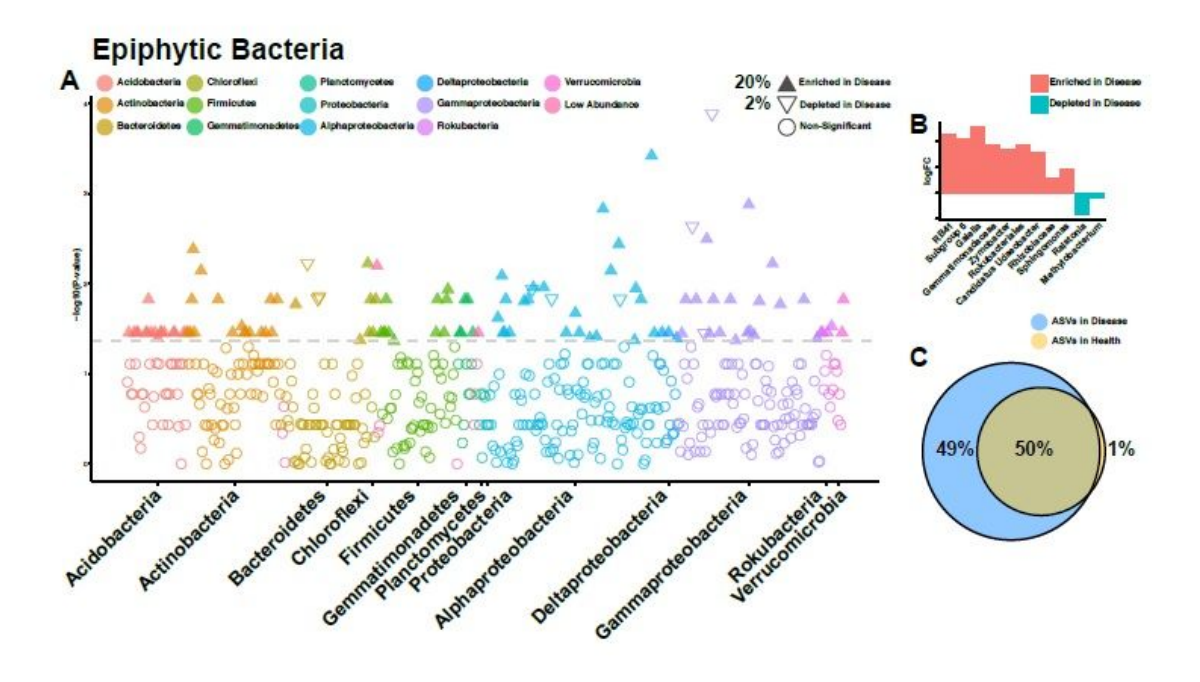
Figure 2

Using alpha and beta diversity to compare the phyllosphere microbiomes between the diseased and healthy groups of leaves. Richness (observed ASVs) and Pielou's Evenness indices were conducted to characterize the alpha diversity and analyzed in Kruskal-Wallis to test for differences. Unconstrained PCoA (for principal coordinates PCo1 and PCo2) with Bray-Curtis metrics was conducted to characterize the beta diversity and analyzed in PERMANOVA to test for differences. Asterisks denote significant differences (*P < 0.05; **P < 0.01; ***P < 0.001) and NS denotes no statistical significance.
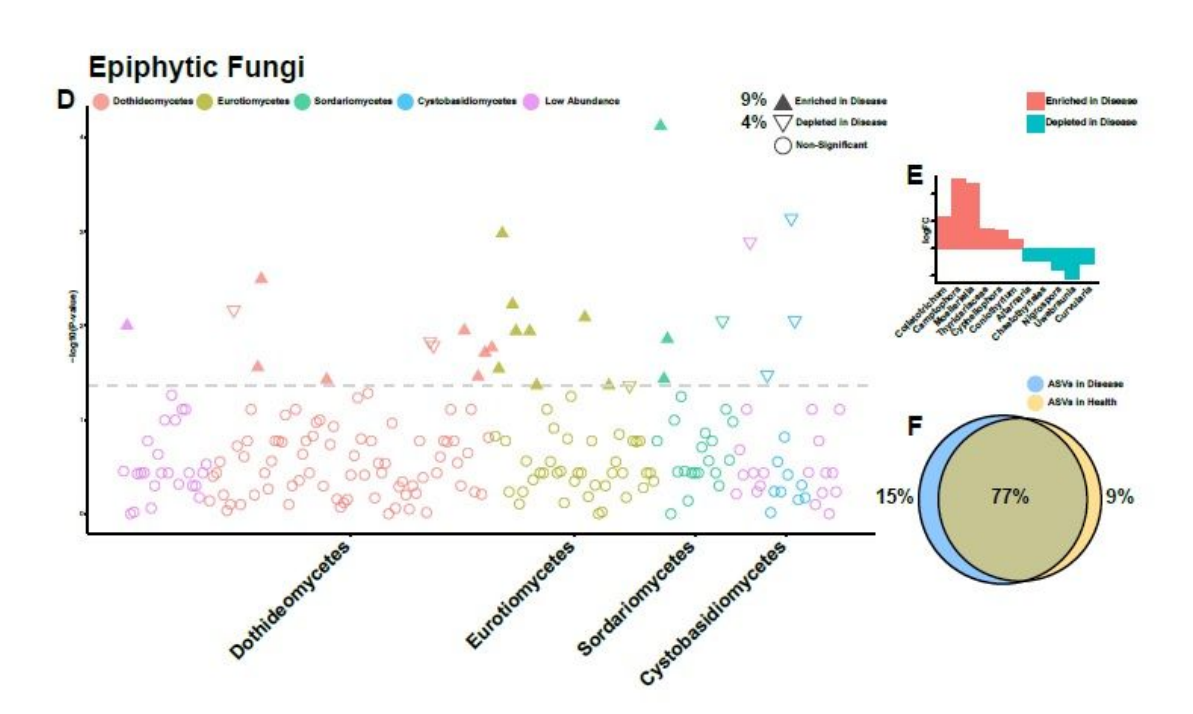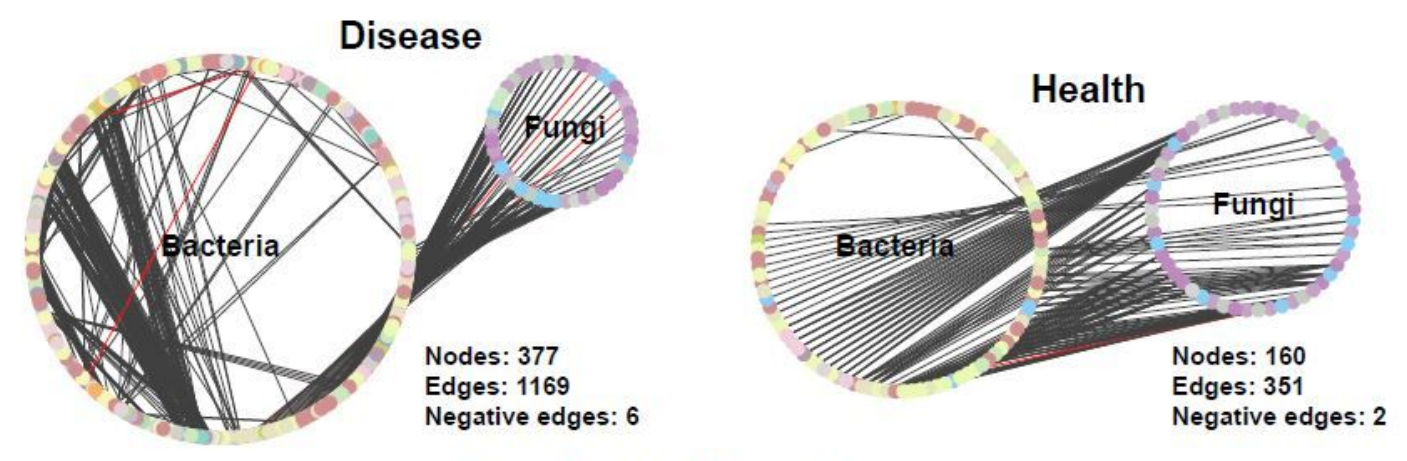
Figure 3

Differential analysis at ASVs or genus level. a, d Manhattan plots showing ASVs enriched or depleted in the diseased group in phyllosphere microbiome. Each circle or triangle represents a single ASV. ASVs enriched or depleted in the diseased group are represented by filled or empty triangles, respectively (ASVs abundance > 0.01%, P < 0.05, FDR < 0.2). c, f Venn diagram depicting the number of ASVs identified in phyllosphere microbiome from the diseased and healthy group. b, e The enriched or depleted genus (if

not annotated to specific genera, using higher-level taxa to represent) in the diseased group of phyllosphere (genus abundance > 0.1%, P < 0.05, FDR < 0.2). Data bars represent the log fold-change (logFC).

Figure 4

Correlation networks for the epiphytic microbiome. Co-occurrence network based on Spearman correlation at ASVs level. Each node represents a single ASV, which was colored based on class level. A connection stands for a statistically significant (P < 0.01) correlation with magnitude > 0.7 (positive correlation, black edges) or < -0.7 (negative correlation, red edges).
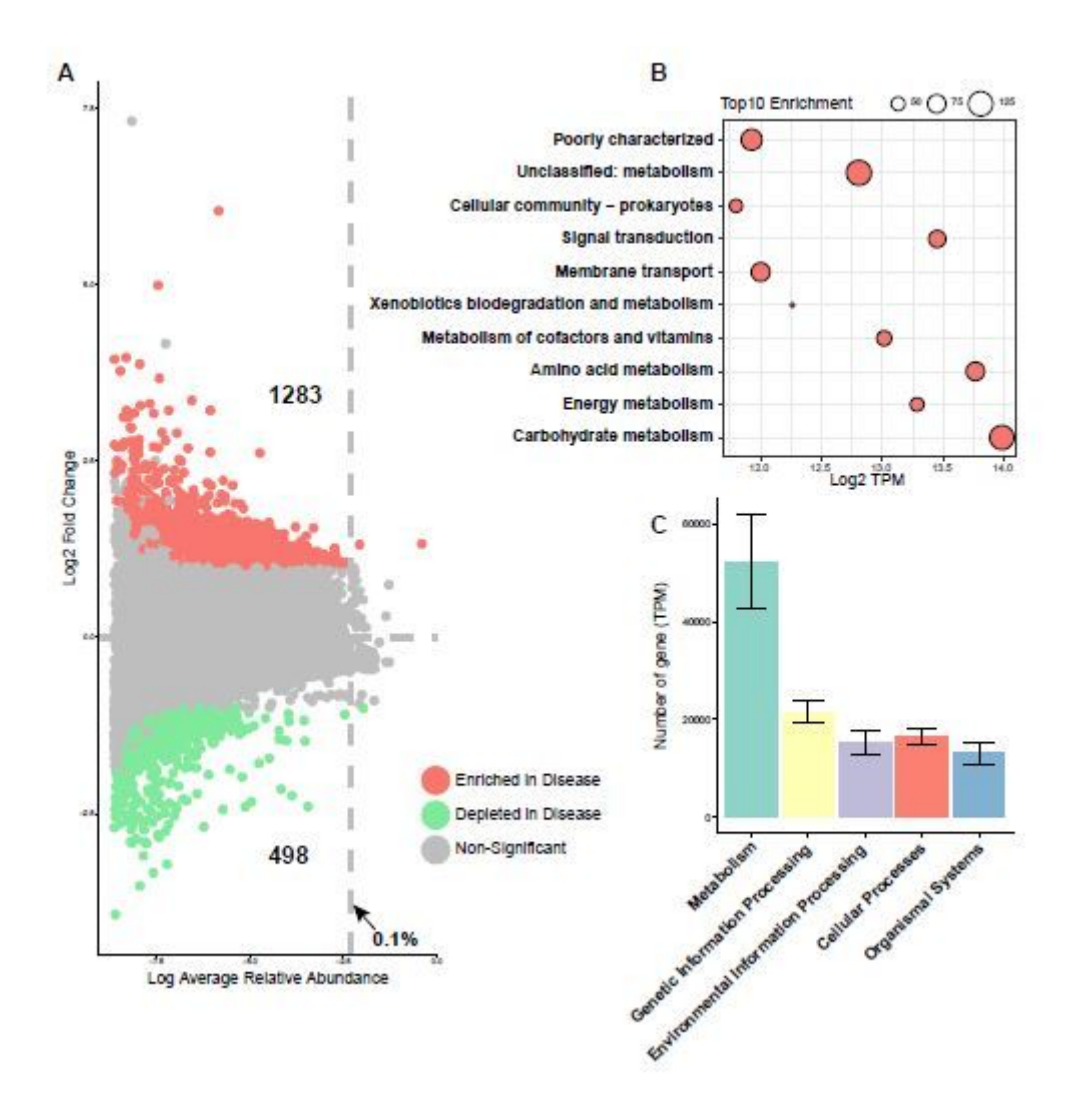
Figure 5

Overview of functional profiling (KEGG) in the epiphytic microbiome. Differentially expressed genes (DESeq2; P < 0.05, FDR < 0.1) at a KO (KEGG Ortholog) and pathway level (b Level 2) between diseased and healthy groups. a Enrichment and depletion of the KOs, fold change > 2 or < -2, respectively. b The number of enriched-KOs in the diseased group involved in KEGG pathway (Level 2). The circle sizes represent the number of enriched-KOs. The X-axis represents the abundance of genes (TPM, log2 transformed) involved in pathway. c Number and type of genes assigned to KEGG pathway (Level 1) in the diseased group. Data bars represent average number of gene (TPM, transcripts per million). Error bars represent 95% confidence intervals.
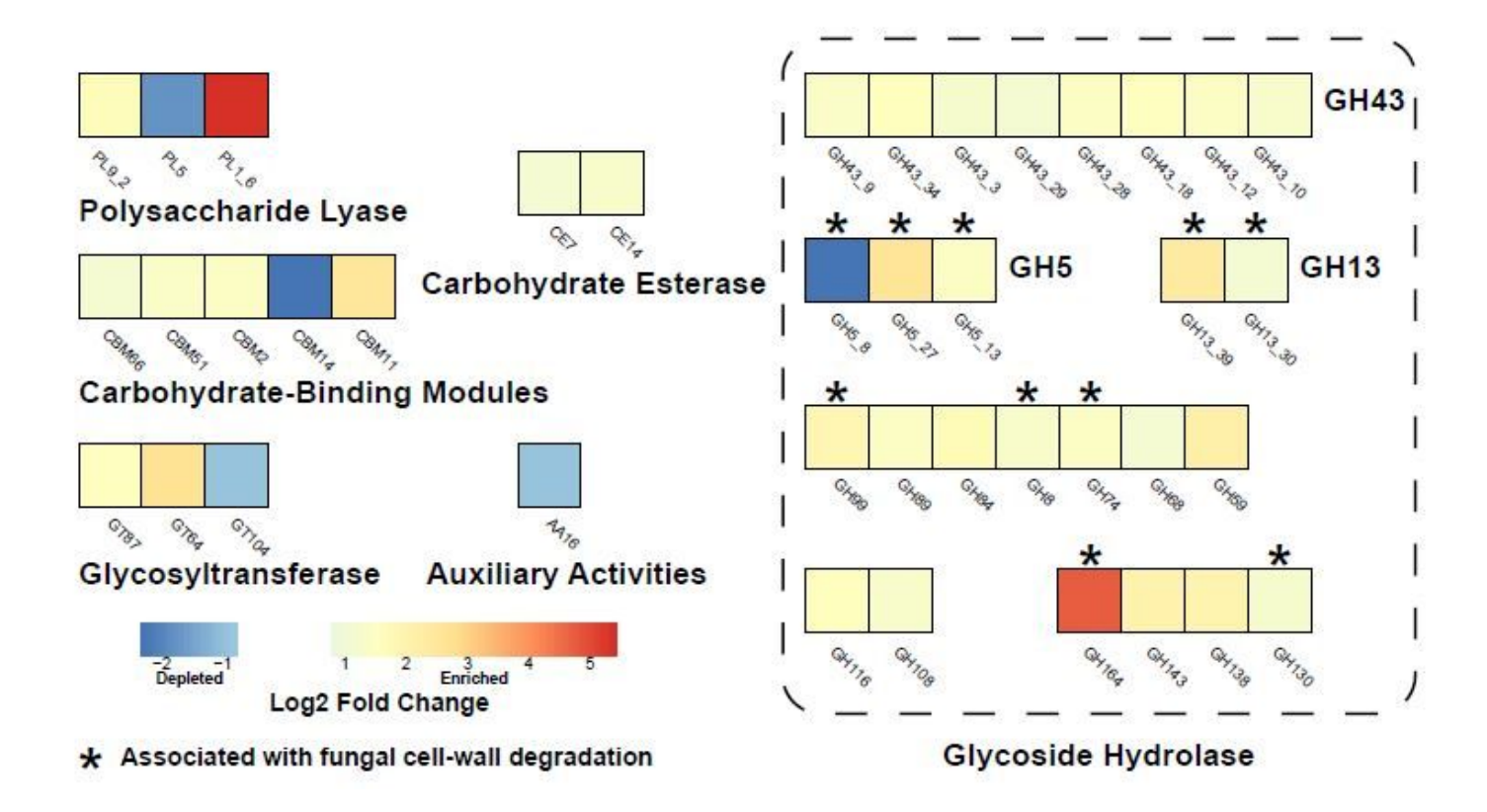
Figure 6

Diversity and distribution of carbohydrate-active enzymes (CAZy) in the epiphytic microbiome. The blocks represent enzyme-related genes that are significantly enriched (Fold Change > 2) or depleted (Fold Change < -2) in the diseased leaves compared with the healthy leaves (DESeq2; P < 0.05, FDR < 0.1).
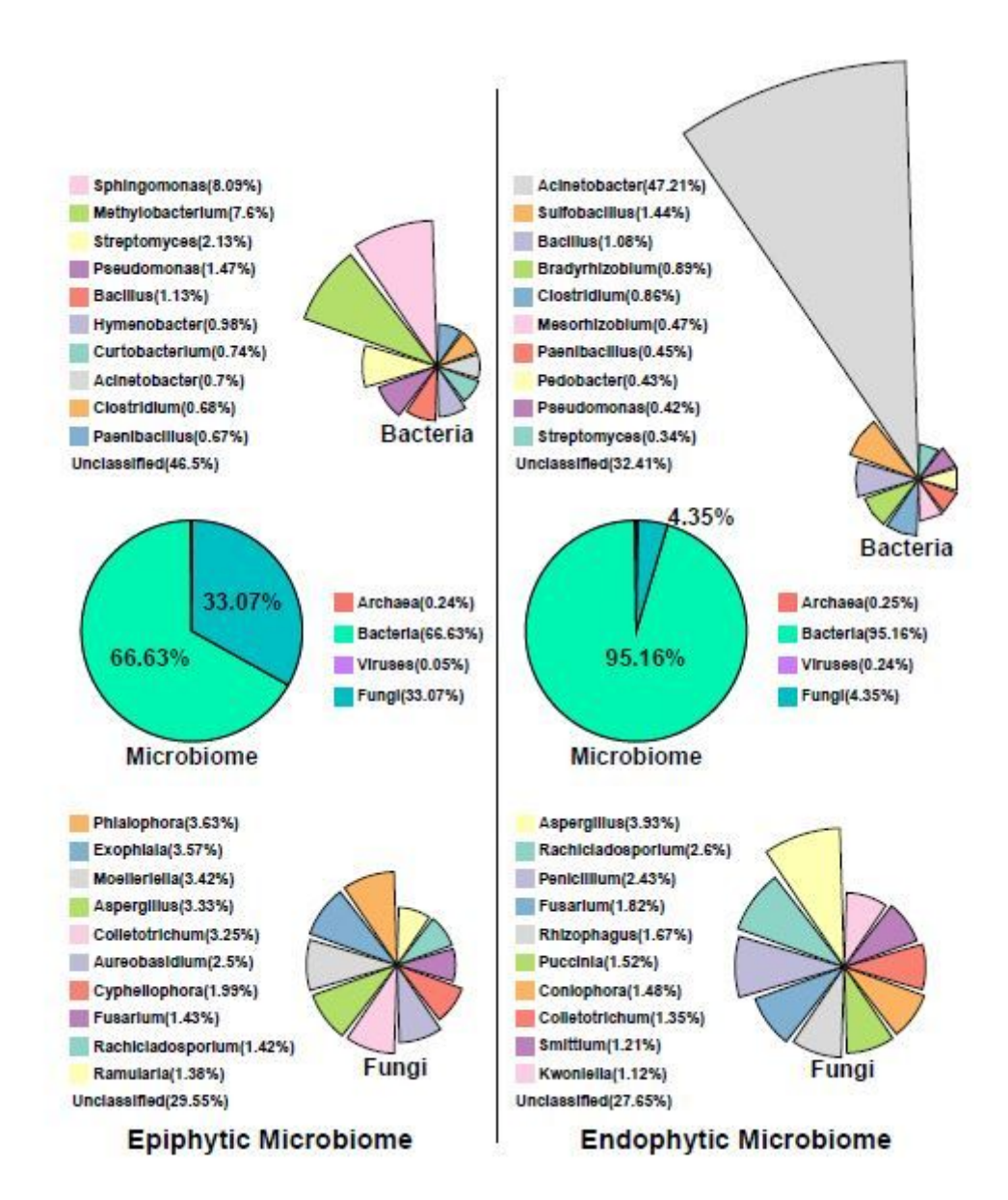
Figure 7

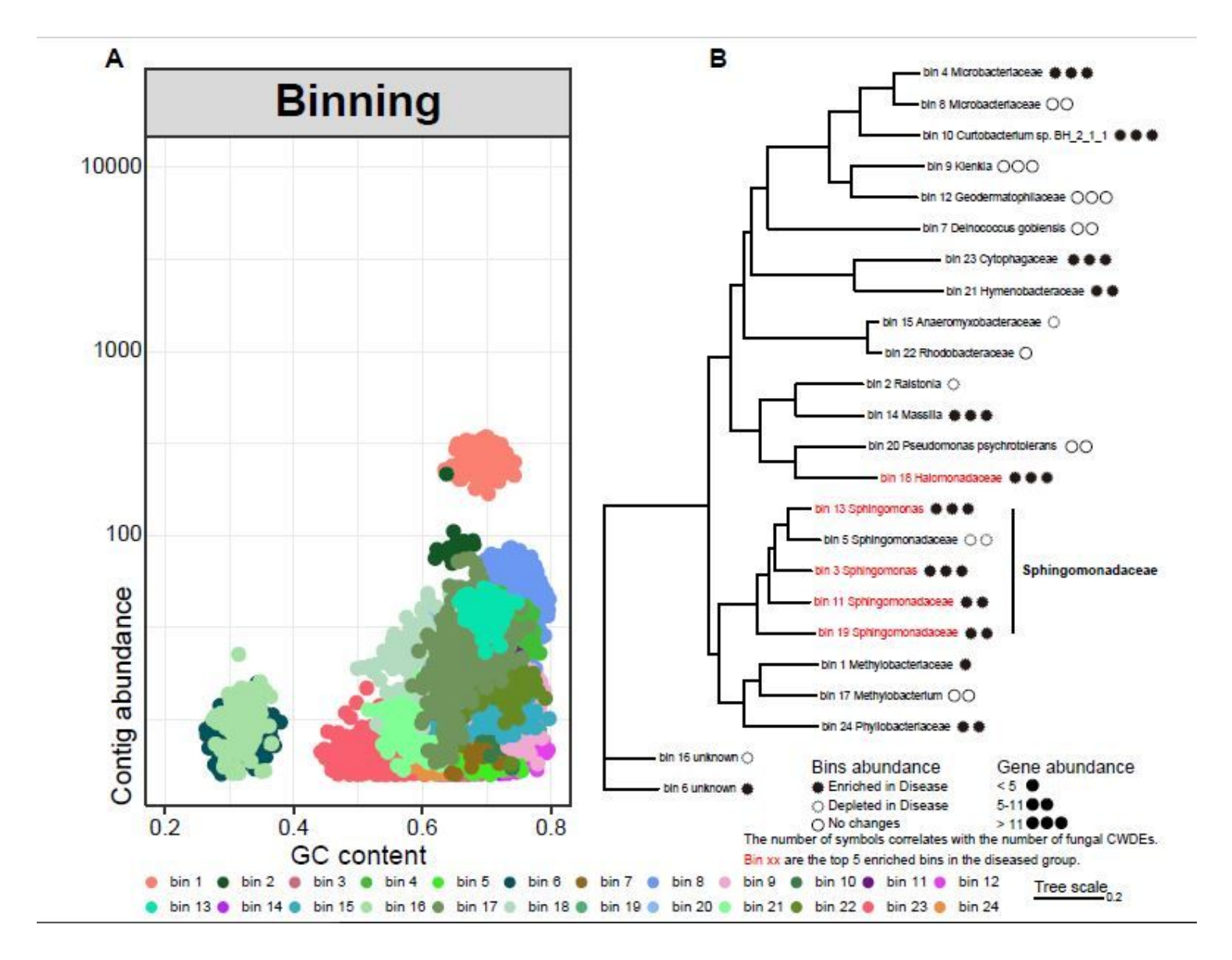Overview of the annotated microbial reads of the phyllosphere microbiome in the diseased leaves.

Figure 8

Binning of the shotgun metagenomic data from the epiphytic microbiome. a Scatterplot representing the distribution of the assembled contigs based on their GC content and abundance. b Phylogenetic tree of the draft genomes (bins, n = 24) from the MAGs (metagenome assembled genomes) data (completeness > 70%, contamination < 10%). The tree was produced from concatenated alignments of up to 400 ubiquitously conserved proteins identified with PhyloPhlAn and used the SGB (species-level genome bins) release to assign to each genome bin its closest SGB. Enrichment and depletion of the bins, fold change > 2 or < -2, respectively. The number of symbols correlates with the number of fungal CWDEs (cell wall-degrading enzymes) based CAZy database.
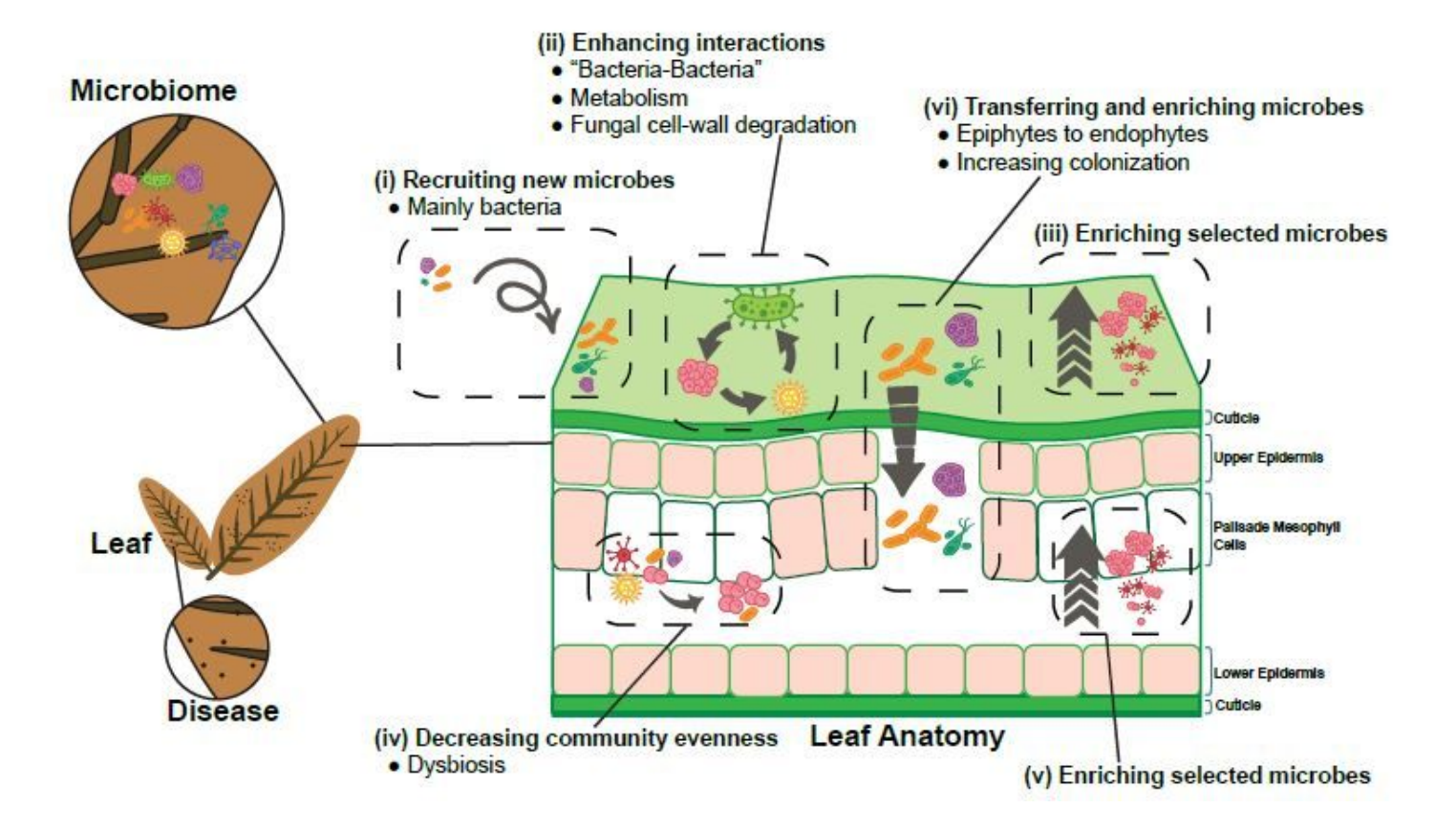
Figure 9

A general conceptual paradigm to describe the different microbial community assembly processes for the phyllosphere microbiome in response to leaf disease. (i) Recruiting new microbes, (ii) enhancing interactions among bacteria and (iii) enriching selected microbes in the epiphytic habitat; (iv) decreasing the microbial community evenness and (v) enriching selected microbes in the endophytic habitat; (vi) transferring and enriching microbes from the epiphytic to the endophytic habitats.

Supplementary Files

This is a list of supplementary files associated with this preprint. Click to download.

- Additionalfile2.xlsx
- Additionalfile1.pdf